Report 7356

GERMANIUM ACCUMULATION-MODE CHARGE-INJECTION-DEVICE PROCESS

T. G. Moore
Aerojet ElectroSystems Company
P.O. Box 296
Azusa, California 91702

June 1981
Final Report for Period September 1980 — June 1981

Prepared for
GODDARD SPACE FLIGHT CENTER
Greenbelt, Maryland 20771

TECHNICAL REPORT STANDARD TITLE PAGE

1. Report No.	2. Government Accession No.	3. Recipient's Catalog No.

4. Title and Subtitle
Germanium Accumulation-Mode Charge-Injection-Device Process

5. Report Date
June 1981

6. Performing Organization Code

7. Author(s)
T. G. Moore

8. Performing Organization Report No.
7356

9. Performing Organization Name and Address
Aerojet ElectroSystems Company
P.O. Box 296
Azusa, California 91720

10. Work Unit No.

11. Contract or Grant No.
NAS5-26318

12. Sponsoring Agency Name and Address G. Lamb, Code 724
Goddard Space Flight Center
National Aeronautics and Space Administration
Greenbelt, Maryland 20771

13. Type of Report and Period Covered
Final report
Sept. 80 - June 81

14. Sponsoring Agency Code

15. Supplementary Notes

16. Abstract

Gallium-doped germanium was found suitable for applications in the detection of far-infrared radiation (FIR). Measurements were made on experimental photoconductors (PCs), accumulation-mode charge-injection devices (AMCIDs), and the SSPC (a switched, sampled PC alternative to the AMCID). Analyses of the results indicated that the SSPC, which had a responsivity near 1.5 amp/watt, is desirable for use in two-dimensional detector arrays.

17. Key Words (Selected by Author(s))	18. Distribution Statement
Infrared, AMCID, Photoconductor, LWIR, Germanium Sampled-switched Photoconductor	

19. Security Classif. (of this report)	20. Security Classif. (of this page)	21. No. of Pages	22. Price*
Unclassified	Unclassified	32	

*For sale by the Clearinghouse for Federal Scientific and Technical Information, Springfield, Virginia 22151.

PREFACE

The objective of the program reported here was to investigate the feasibility of using doped-germanium accumulation-mode charge-injection devices (AMCIDs) as sensors of far-infrared radiation (FIR).

The work began with a literature survey for germanium field-effect-device experience applicable to AMCID construction. It was followed by an experimental program comparing the photoconductor (PC), the AMCID, and the SSPC, a switched sampled photoconductor alternative to the AMCID.

Gallium-doped germanium was found suitable for FIR applications, and the PC and SSPC showed responsivities near 1.5 amperes per watt. The PC would be useful in a single-element detector, but the AMCID or the SSPC would be needed for two-dimensional arrays because of their economy in amplifier requirements. The slow-rise characteristic of the AMCID and the comparatively simpler SSPC fabrication lead to a recommendation that the SSPC be considered for use in detector arrays.

TABLE OF CONTENTS

FIGURES

FIGURES (CONT.)

ABBREVIATIONS

AESC	Aerojet ElectroSystems Company
AMCID	accumulation-mode charge-injection device
BP/Q/BP	black polyethylene/quartz/black polyethylene (layered filter)
CCD	charge-coupled device
CID	charge-injection device
CTD	charge-transfer device
CVD	chemical-vapor deposited (deposition)
dc	direct current
FET	field-effect transistor
FIR	far infrared radiation
IGFET	insulated-gate FET
IR	infrared
JFET	junction FET
LED	light-emitting diode
LHe	liquid helium
LN_2	liquid nitrogen
MOS	metal-oxide semiconductor
MOSFET	metal-oxide-semiconductor field-effect transistor
NASA	National Aeronautics and Space Administration
PC	photoconductor
ph	photons, as in ph/cm^2-sec

ABBREVIATIONS (CONT.)

RC	resistance-capacitance product
Ref.	reference
RMS	root mean square
S/H	sample and hold (device)
SSPC	switched, sampled photoconductor
TM	technical manual
ϕ	equivalent flux
ϕ_s	signal flux

Section 1

INTRODUCTION AND SUMMARY

Doped-germanium photoconductors are of considerable interest for the detection of far-infrared radiation (FIR) because their long-wavelength extrinsic limit can extend well beyond that of any silicon material. In addition, the need for techniques for the integration and sampling of low-level signals in large arrays has focused attention on the accumulation-mode charge-injection-device (AMCID) architecture. In the program reported here Aerojet has investigated the feasibility of a doped-germanium AMCID for FIR sensor applications. To this end a literature search was conducted to determine previous experience with field-effect types of devices fabricated on germanium that might be relevant to AMCID construction. Measurements were made on experimental gallium-doped germanium photoconductors (PCs), and on mercury-doped germanium AMCID detectors, as well as on an alternative to the AMCID: the switched, sampled photoconductor (SSPC). Responsivity measurements for the PC and SSPC yielded values near 1.5 amp/watt. It was concluded that both the AMCID and the SSPC should satisfy FIR requirements, with the SSPC the recommended structure.

Section 2

LITERATURE SEARCH

A search of the open literature was conducted to determine the current state of the art in relevant germanium MOS technology. Use was made of the Lockheed Space and Missile Systems Information Retrieval Service, "DIALOG", and of the National Aeronautics and Space Administration (NASA) file. The DIALOG files accessed were as follows:

File No.	Name	Dates Covered
6	NTIS	1964-1980
8	COMPENDEX	1970-1980
12	INSPEC	1969-1977
13	INSPEC	1978-1980

The key words and abbreviations associated with this search were germanium (Ge), charge-coupled device (CDD), charge-transfer device (CTD), charge-injection device (CID), junction field-effect transistor (JFET), metal-oxide-semiconductor field-effect transistor (MOSFET), insulated-gate field-effect transistor (IGFET), and field-effect transistor (FET).

Only seven articles of interest to this program were obtained in the search. It is apparent that little information on this subject has appeared in the open literature. Two Aerojet reports of direct interest are also included in the list of references following the text.

Chang and Yu (Ref. 1) made germanium insulated-gate FETs using pyrolytic SiO_2 deposited at 740°C as the insulator. They observed low-frequency hysteresis but made no estimates of slow-surface-state densities in their devices. Interface properties of alumina-germanium MOS transistors were studied by Iwauchi and Tanaka (Ref. 2), who deposited Al_2O_3 on antimony-doped germanium by dc reactive sputtering. They observed surface-state densities of 10^{11}/eV-cm^2 and electron-capture cross sections about 2 orders of

magnitude smaller than those typically observed for a silica-silicon interface. Schroder (Ref. 3) pointed out that the germanium dioxide insulator reacts with Ge above 550°C to form the volatile compound GeO_2 as the gate insulation. Consequently, he used chemical-vapor-deposited (CVD) SiO_2, and also achieved surface-state densities of 10^{11}/eV-cm^2. Wang and Gray (Ref. 4), likewise using CVD SiO_2, measured a somewhat higher surface-state density of 2.5×10^{11}/eV-cm^2. Don, et al. (Refs. 5 and 6) analyzed the weak inversion mode in germanium MOSFETs fabricated with SiO_2 as the gate insulation on 0.5 ohm-cm p-type germanium. They too achieved surface-state densities of 10^{11}/eV-cm^2.

Haller (Ref. 7) has studied gallium-doped germanium for use in FIR detectors. Particularly pertinent to this current effort were techniques he described to electrode the germanium using boron implants under titanium-gold sputtered contact metalization.

Section 3

DEVICE FABRICATION

Sample devices were fabricated in both photoconductive and AMCID configurations. Germanium doped with 3 x 10^{14} gallium atoms per cubic centimeter was used for the extrinsic PC detectors, and mercury-doped germanium was used for the test AMCIDs.

The PC samples were made of wafers that were sawed from a Ge:Ga boule and were lapped and polished to a thickness of approximately 1 mm. Both surfaces of each wafer were ion-implanted with boron at 60 keV to a concentration of 4 x 10^{14} cm^2.

The implanted slices were heat-treated in dry argon for 30 minutes at 250°C, and were subsequently electroded by vacuum deposition of 200 angstroms of titanium, followed by 6000 angstroms of gold. The finished devices had an interelectrode spacing of 1 mm, an active area of 1 by 4 mm, and an absorption depth of 4 mm.

Three such devices were mounted, with indium solder, on a copper header. The header was epoxied to a heat sink that could be bolted to the cold finger in the test vessel. The header was insulated so that the bias could be applied to the detector directly or the detector could be grounded, as the testing required. These detectors could then be used in the switched mode by replacing the load resistor with a switching MOSFET for use in signal readout.

Mercury-doped germanium was selected for the test AMCIDs both because of its ready availability and for the attendant relaxed test requirements, especially with regard to temperature. The Ge:Hg wafers were lapped and polished on both sides to a thickness of 0.25 mm. A transparent electrode was ion-implanted on one side. Boron was implanted at 60 keV and a concentration of 1 x $10^{13}/cm^2$. The wafers were heat-treated at 400°C for 30 minutes,

to provide a 1-micrometer-deep layer at a density of 10^{17} atoms/cm^3. The plasma-absorption edge in this layer should be near 60 micrometers, which is well beyond the response cutoff of Ge:Hg.

On the other side of the wafers, an insulated layer, 2000 angstroms thick, was formed to serve as the gate oxide. Several insulator materials were investigated, including GeO_2, Al_2O_3, SiO_2, and polyimide. In all cases except Al_2O_3, the dielectric layer failed to keep the gates sufficiently insulated from the substrate. Consequently, the final AMCID measurements were made on devices using Al_2O_3.

Gold was vacuum-deposited on both sides of the wafer for contact metalization. On the transparent-electrode side, holes were opened in the gold layer, using photolithographic techniques, and islands directly opposite the holes were etched for gate electrodes. The active area over the transparent electrode was 1 mm square.

The AMCID configuration is shown in Figure 1. The two metal patterns on the wafer are configured identically but are of opposite field. The particular configuration is not significant, but merely resulted from the use of a convenient, existing set of photomasks.

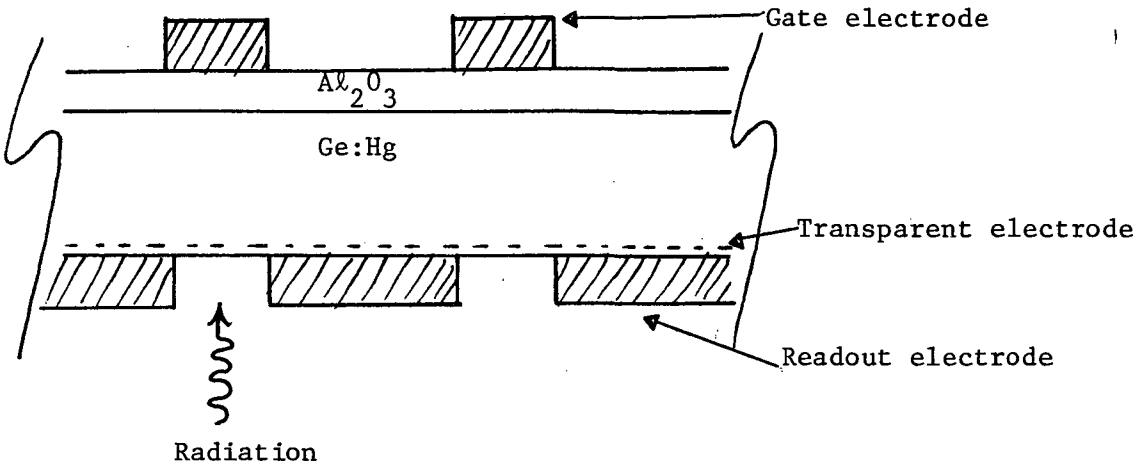

A. Cross Section

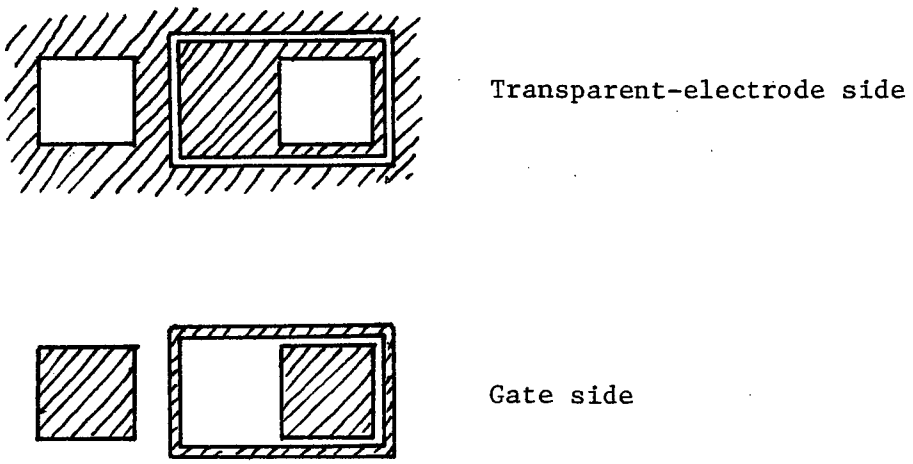

b. Electrode Pattern

FIGURE 1 AMCID CONFIGURATION

Section 4

PHOTOCONDUCTOR TESTS

Measurements were made on detectors fabricated of Ge:Ga operating both the standard photoconductor mode and in the switched sampled photoconductor (SSPC) mode. Infrared optical signals applied to the detector originated at a light-emitting diode (LED) source. The LED was calibrated against a blackbody at high background.

The test configuration is shown in Figure 2. The radiation from a 500 K blackbody, modulated by a 300 K chopper, entered the test cryostat through a quartz window and then passed through a cooled filter made of three components: two 4-mil-thick black polyethylene (BP) films sandwiching a 1-mm-thick quartz (Q) window (i.e., BP/Q/BP). This is the same filter as that used by Yee in the work reported in Ref. 8. Each detector's response to the LED signals was then compared with its response to the blackbody, and an "equivalent flux" in the spectral region from 74 to 125 micrometers was thereby established for the LED.

Measurements were made on the Ge:Ga detectors at temperatures ranging from 3.1 to 4.5 K. These temperatures were obtained by pumping over the liquid-helium reservoir. The temperature of the LHe as measured by vapor pressure was reduced to 1.9 K, but the sample temperature as measured by a calibrated carbon resistor was limited to 3.1 K. The test setup is shown schematically in Figure 3.

Response is plotted against bias voltage for the three photoconductors in Figure 4. Here the equivalent flux (ϕ) is 9.3×10^{-11} W/cm^2. The signal-to-noise ratio improves up to a bias of 0.3 V and then drops off. The tests were made at a bias of 0.4 V because the higher signal was advantageous and the signal-to-noise ratio was degraded only slightly.

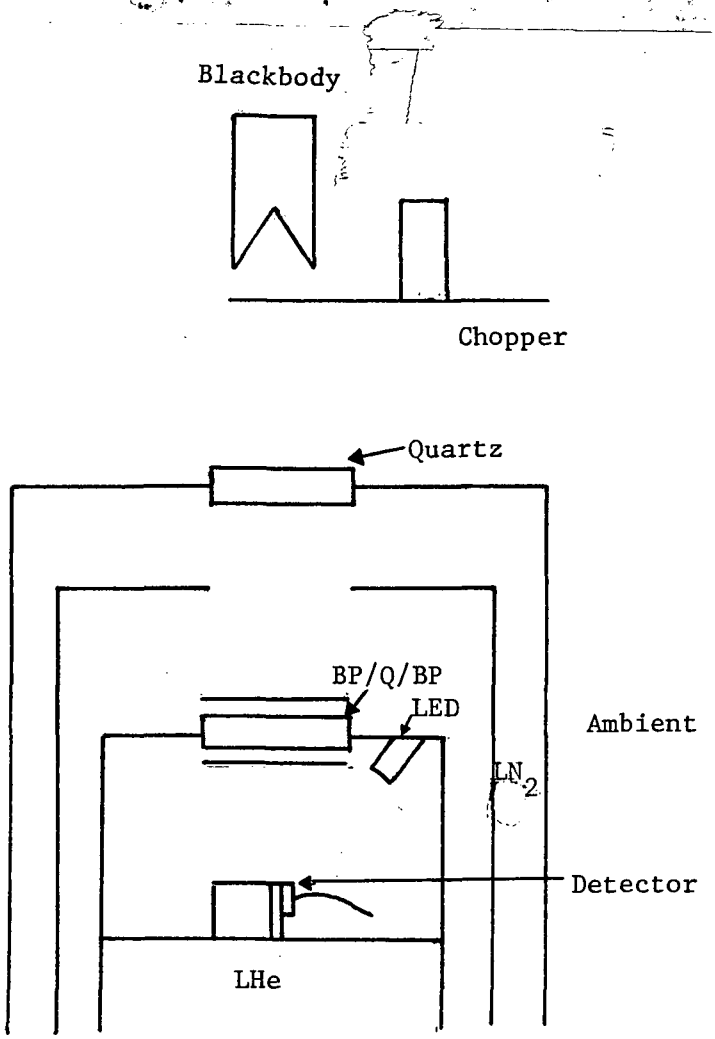

FIGURE 2 TEST CONFIGURATION

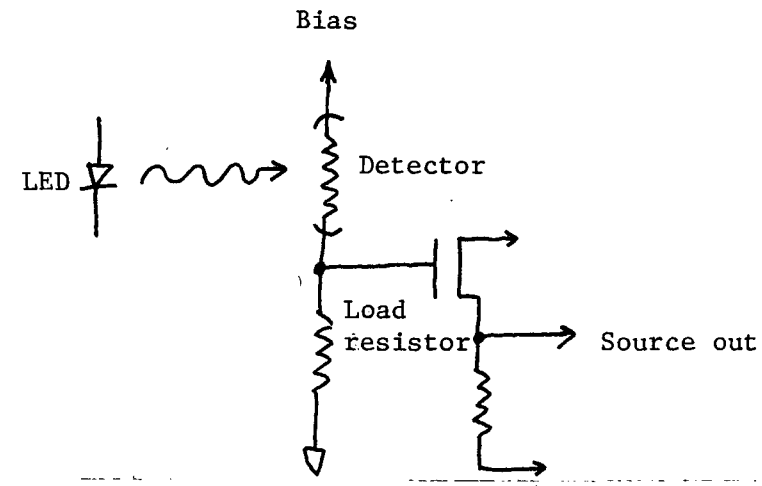

A. Standard Photoconductor

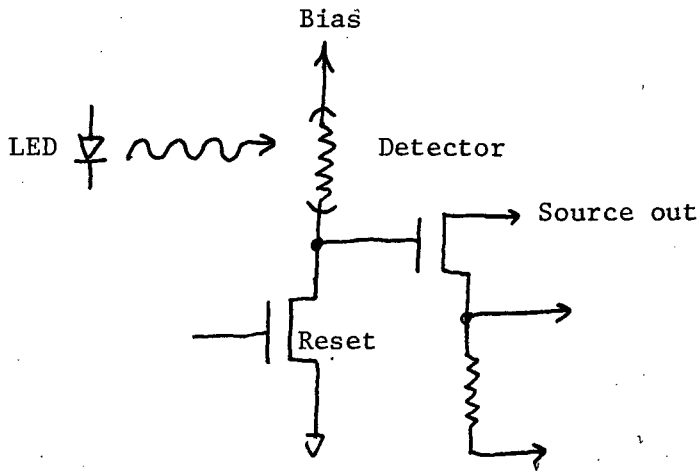

B. Switched, Sampled Photoconductor

FIGURE 3 TEST SETUP, SCHEMATIC

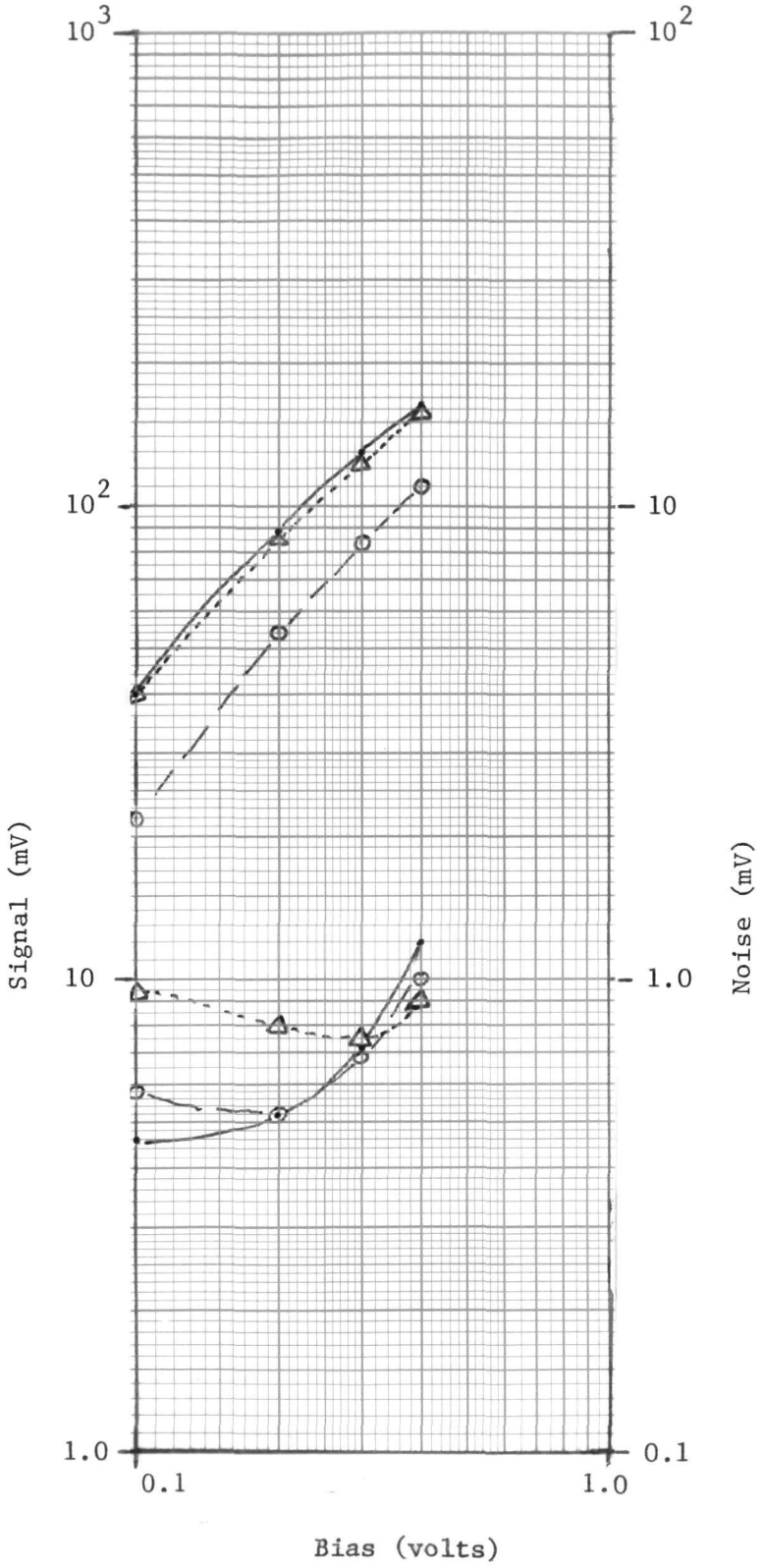

FIGURE 4 PC SIGNAL AND NOISE VS BIAS, $\phi = 9.3 \times 10^{-11}$ W/cm^2

Figures 5, 6, and 7 show the noise spectrum as a function of bias and temperature. The data were smoothed by removing the noise spikes due to 60 Hz and its harmonics. The amplifier bandwidth was approximately 40 Hz which may be seen in the 0.3 V bias curve in Figure 5. Below about 10 Hz there is some excess low-frequency noise probably due to contacts. At the lower bias the detector noise is seen to drop into the system noise.

Figure 8 summarizes the noise at 10 Hz as a function of temperature and bias voltage. At the higher temperature (4.5 K), the noise is independent of bias voltage below 0.4 V. The detector response due to a square-wave infrared (IR) signal at 10 Hz is shown in Figure 9. The rise time is about 4.5 msec, which corresponds to the resistance-capacitance (RC) time constant of the load resistor (1×10^9 ohms) and the input capacitance ($\sim$4 pF). The equivalent signal flux was 1.9×10^{-10} W/cm^2. The current responsivity for this detector is 1.5 amp/watt, which corresponds to measurements made elsewhere on Ge:Ga detectors (e.g., Refs. 7,8).

The standard photoconductor may be converted to a switched sampled photoconductor by replacing the load resistor with a reset MOSFET switch, as shown in Figure 3B. The detector is biased as before, but the detector current is allowed to charge the input capacitance of the source follower during an "integration" period. During integration the reset switch is open. At the end of the integration period, the charge on the input is sampled, the reset transistor is momentarily turned on to discharge the input, and a second sample is taken. The difference between these two correlated samples represents the accumulated signal.

The detector used to obtain the square-wave response shown in Figure 9 was set up as an SSPC, and Figures 10 and 11 show the resulting waveforms for various integration times at the same signal flux and chopping frequency as for the PC. The sample frequency (reciprocal of integration time) varied from 16 to 128 times the signal frequency.

The signal level was found to be a sublinear function of the integration time, as plotted in Figure 12 for frequencies of 10 and 100 Hz. At 100 Hz, the signal is linear below an integration time of 1 millisecond for

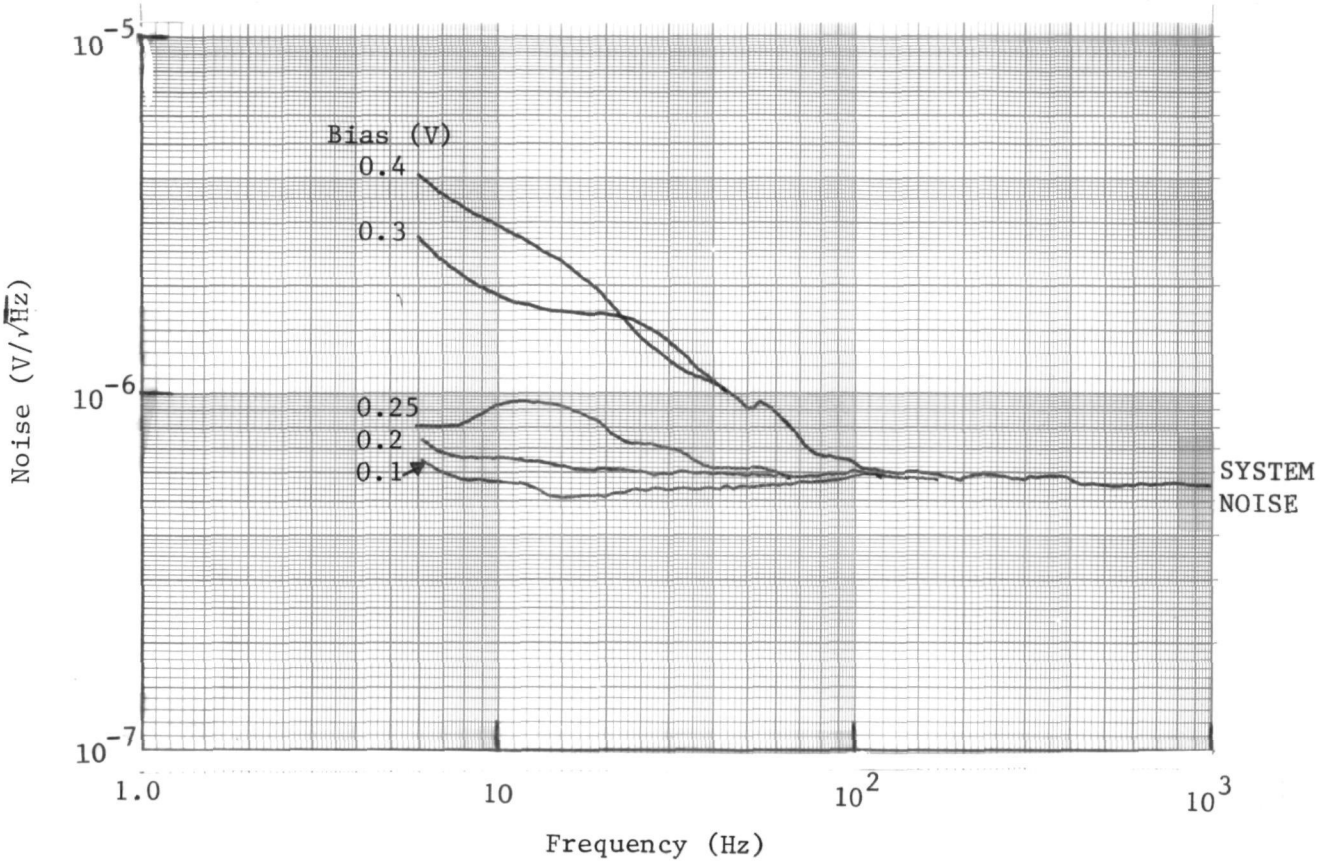

FIGURE 5 PC NOISE SPECTRUM AT 3.2 K

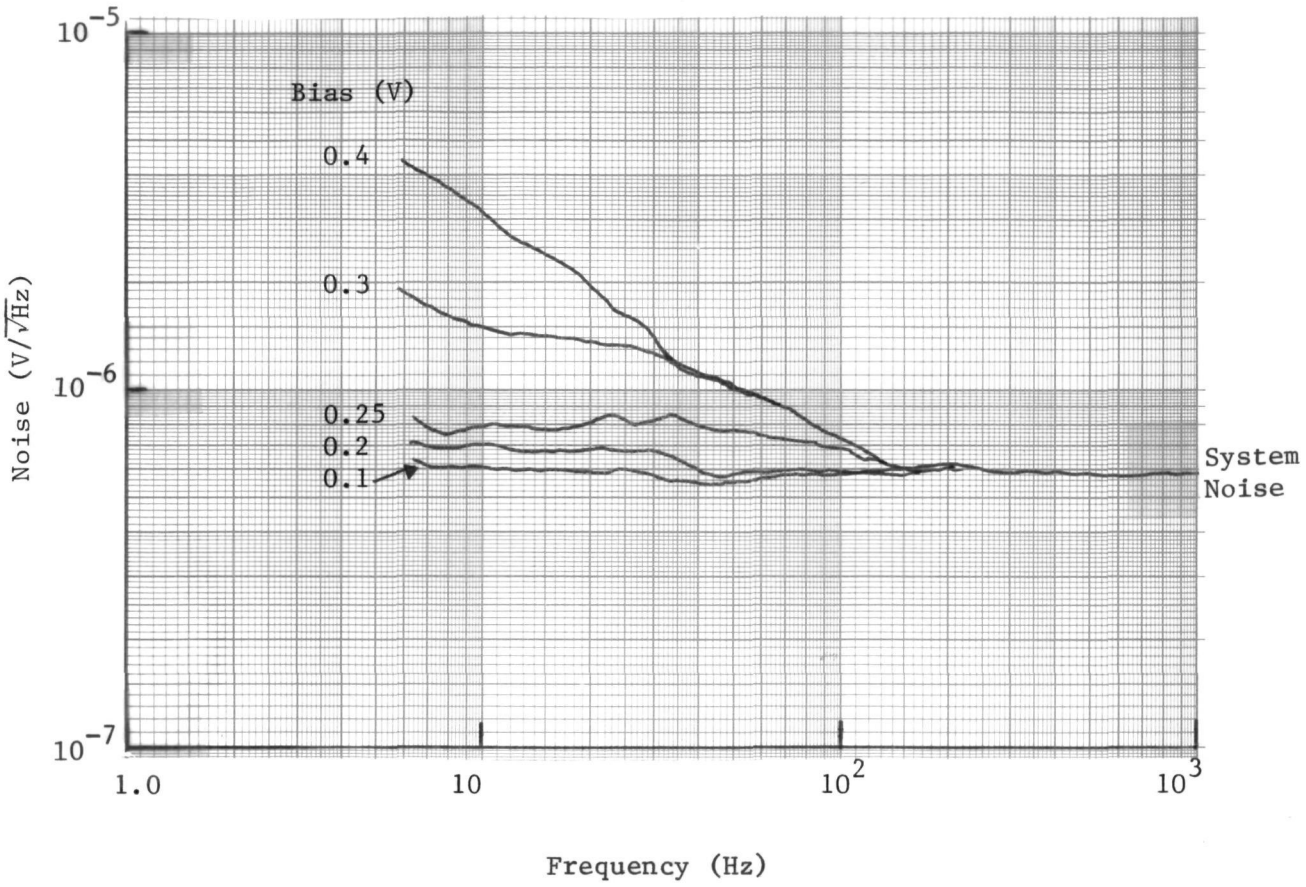

FIGURE 6 PC NOISE SPECTRUM AT 4.0 K

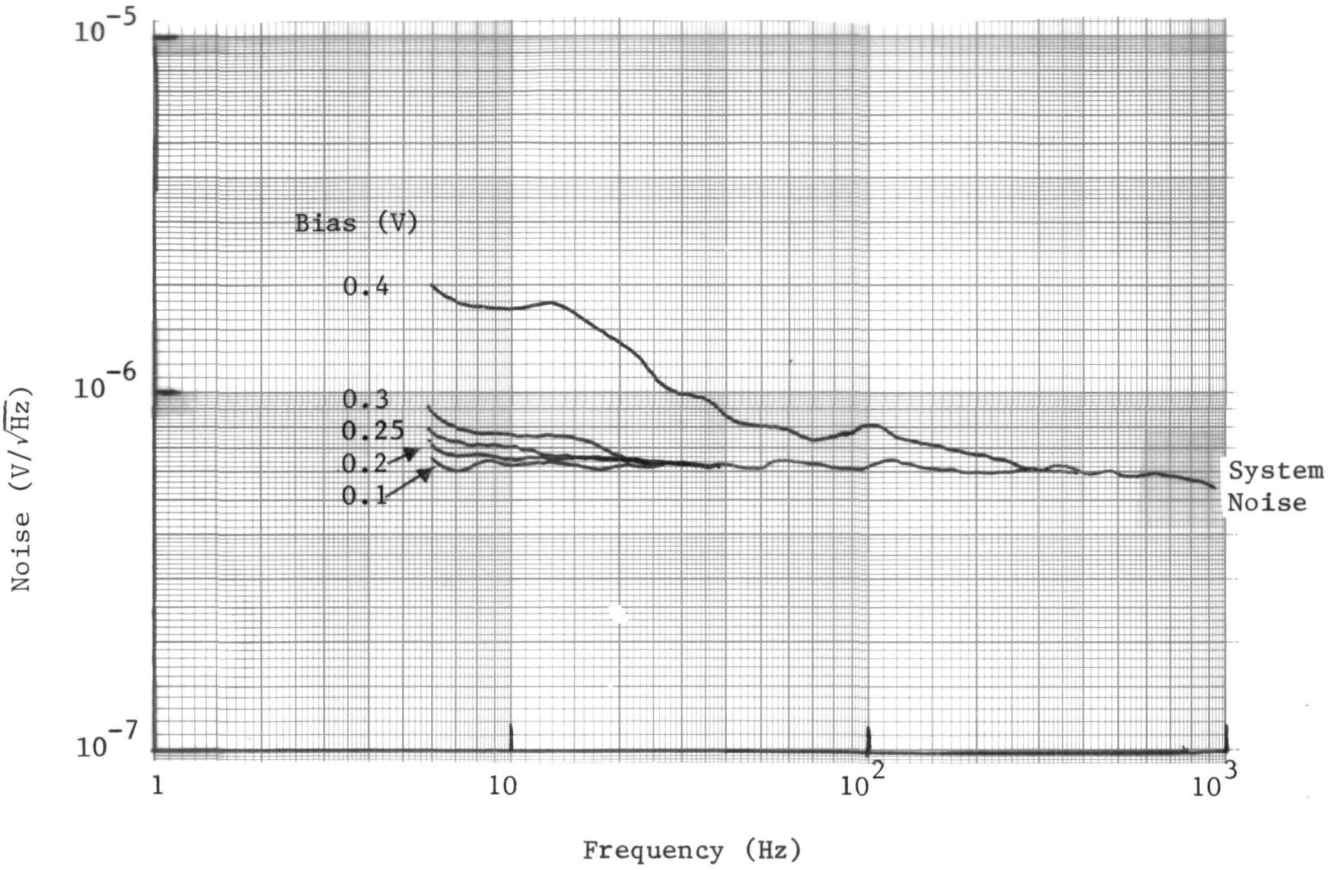

FIGURE 7 PC NOISE SPECTRUM AT 4.5 K

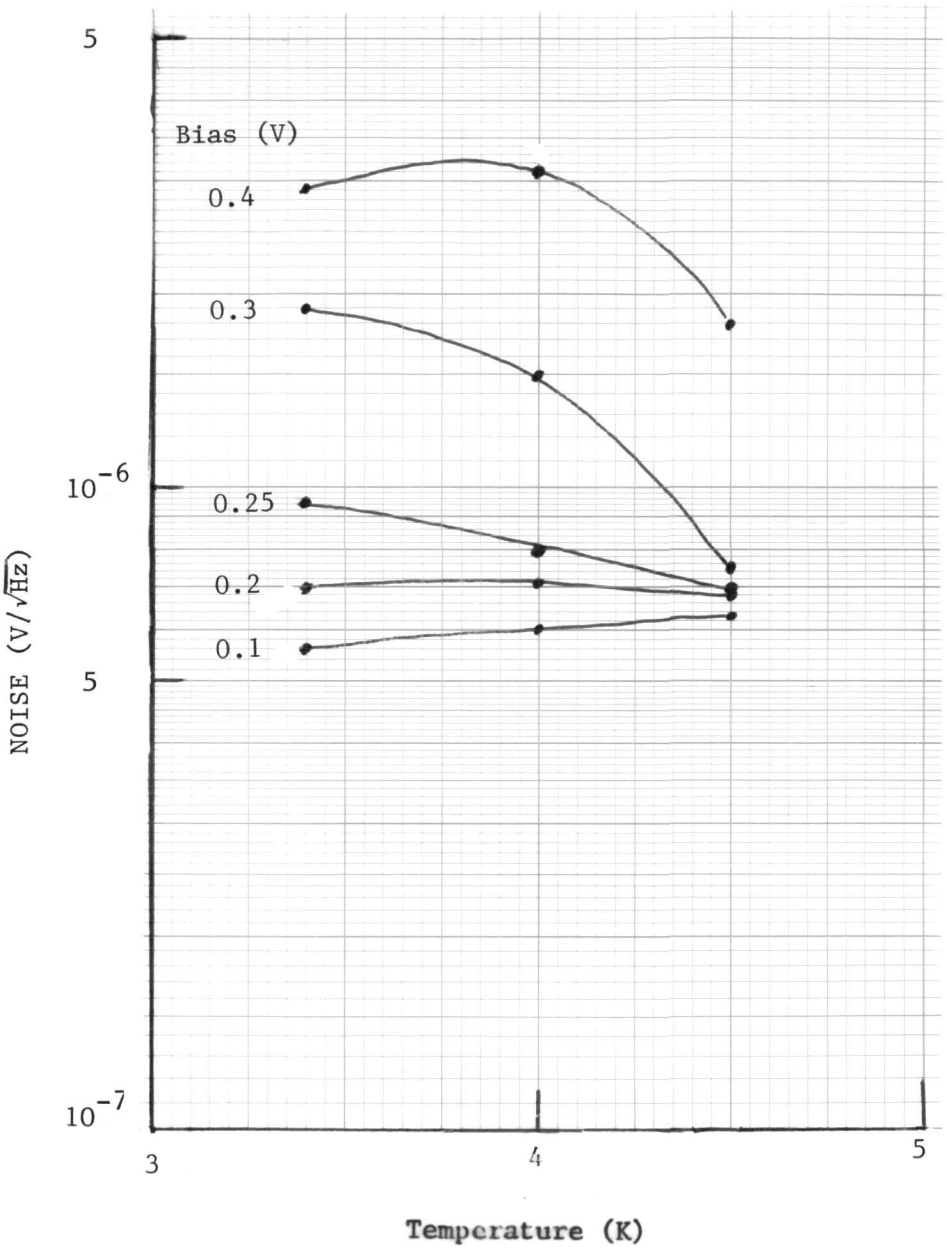

FIGURE 8 PC NOISE VS TEMPERATURE

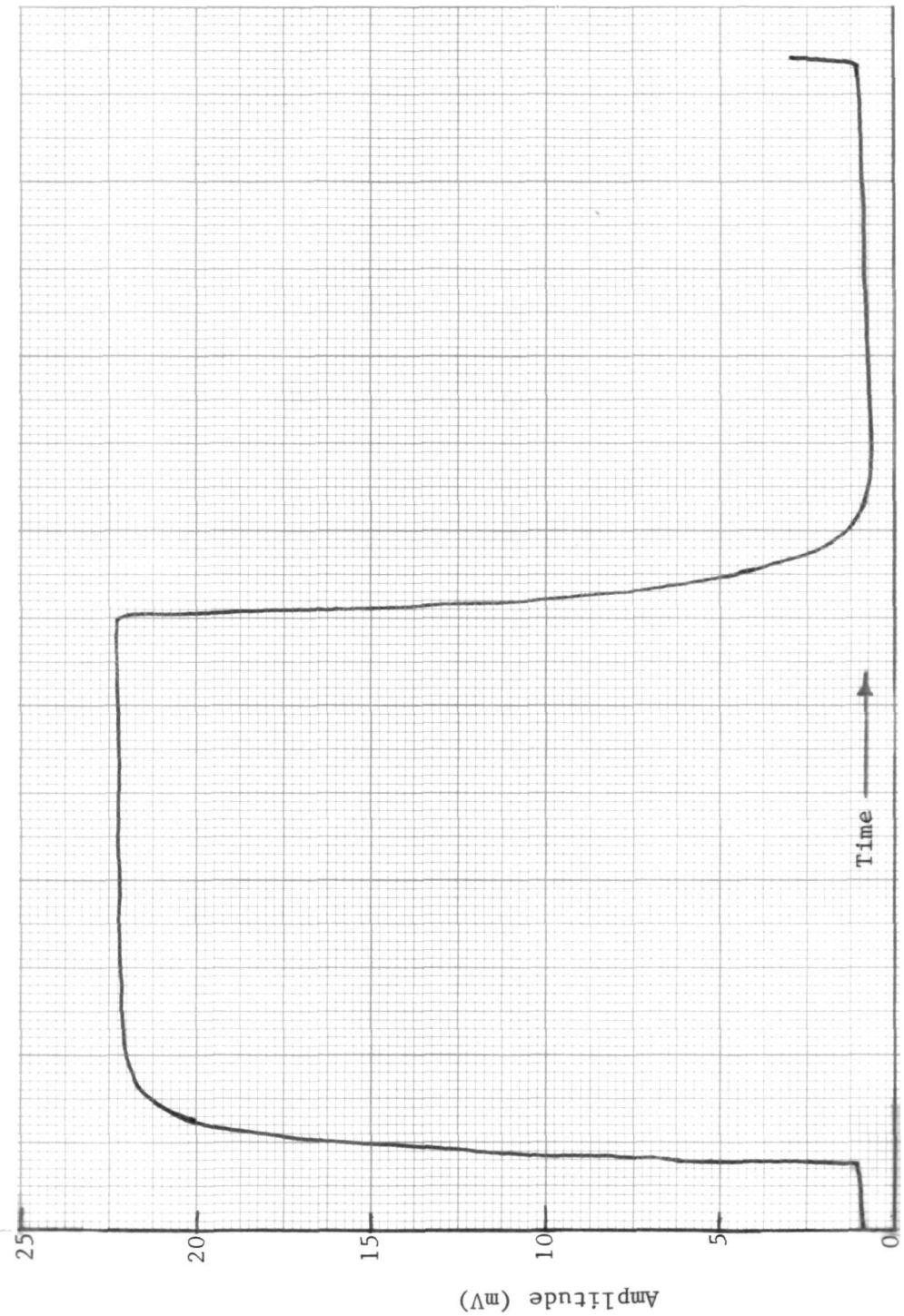

FIGURE 9 PC SQUARE-WAVE RESPONSE AT 10 Hz

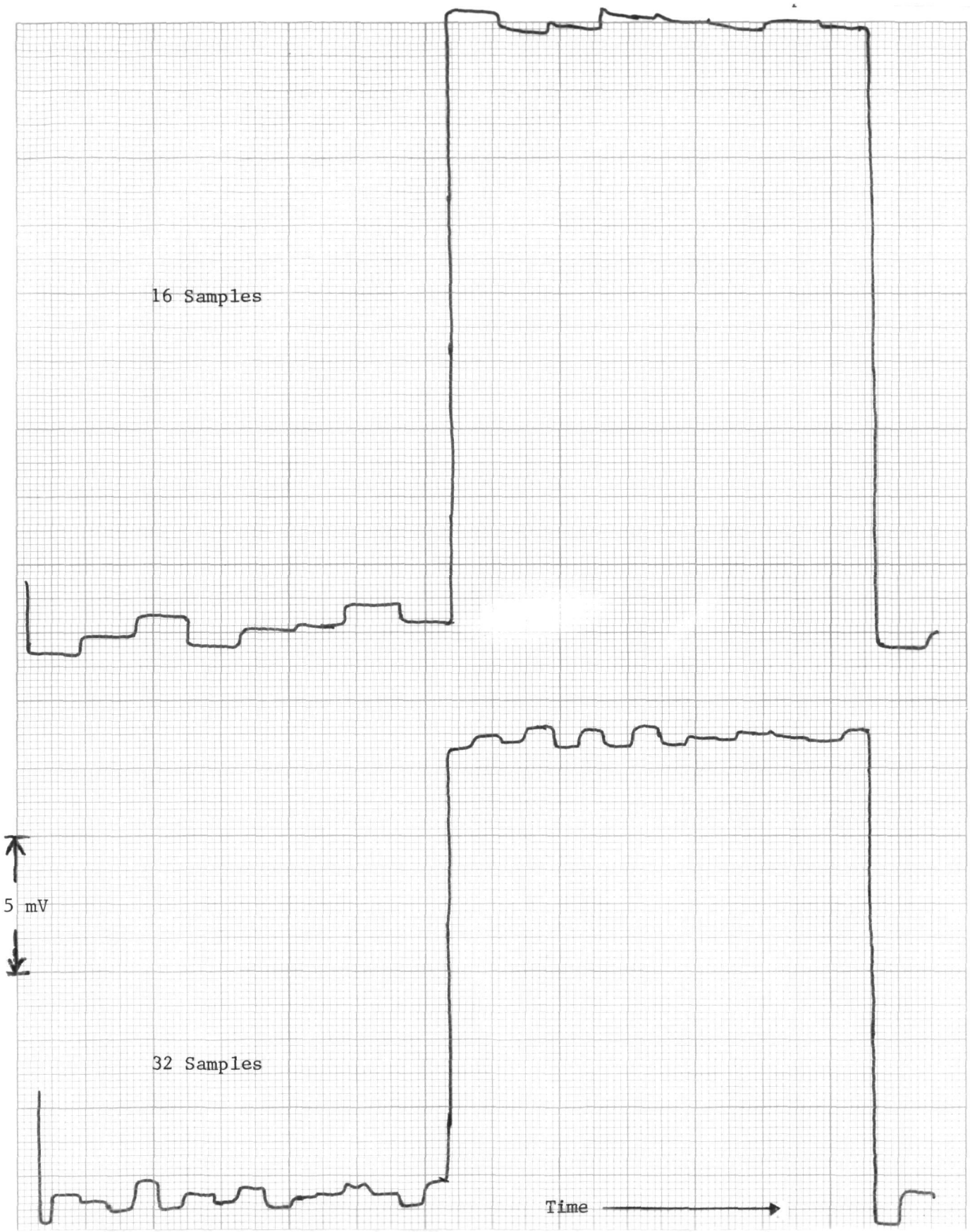

FIGURE 10 SSPC SQUARE-WAVE RESPONSE AT 10 Hz FOR 16 AND 32 SAMPLES

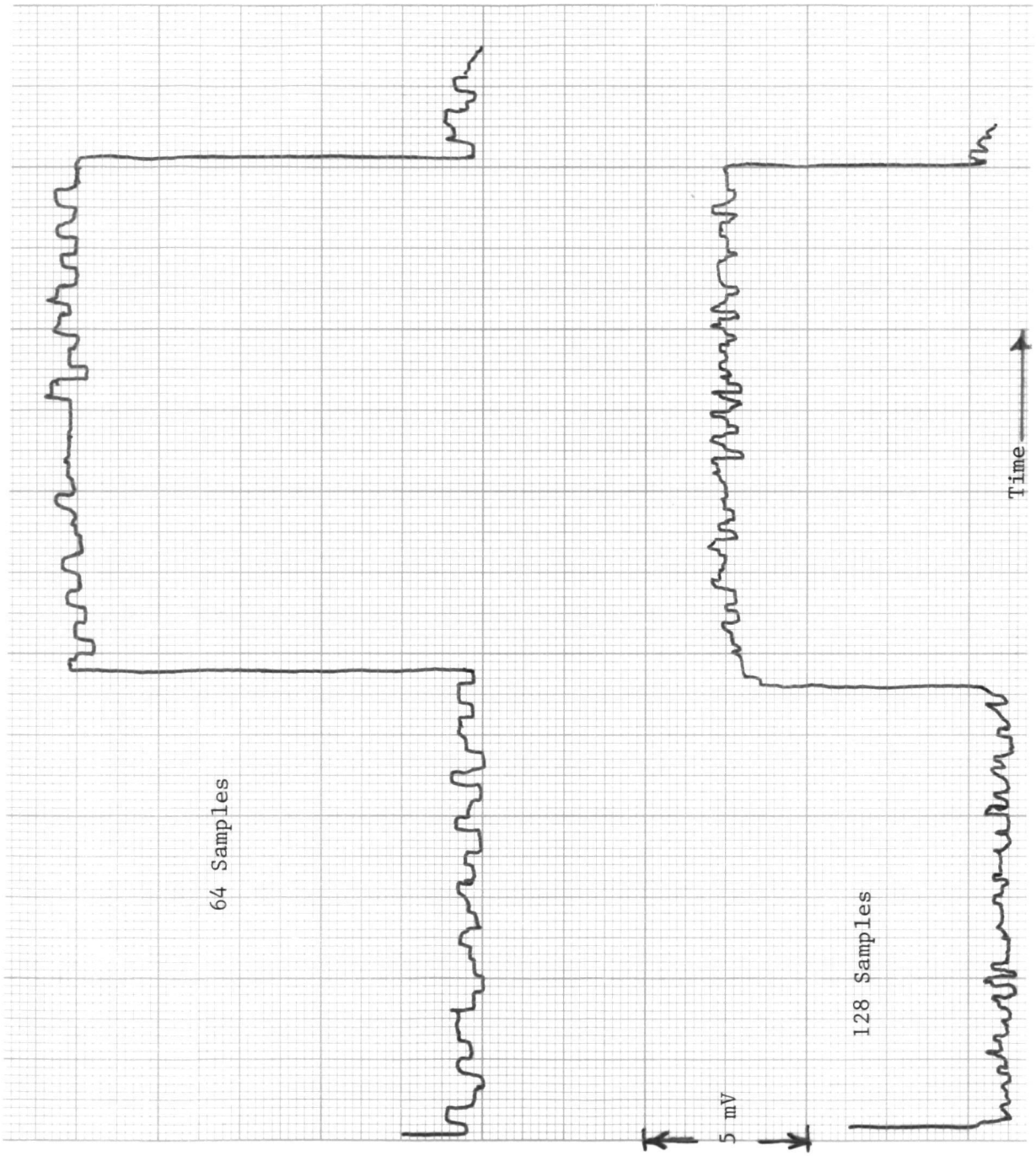

FIGURE 11 SSPC SQUARE-WAVE RESPONSE AT 10 Hz FOR 64 AND 128 SAMPLES

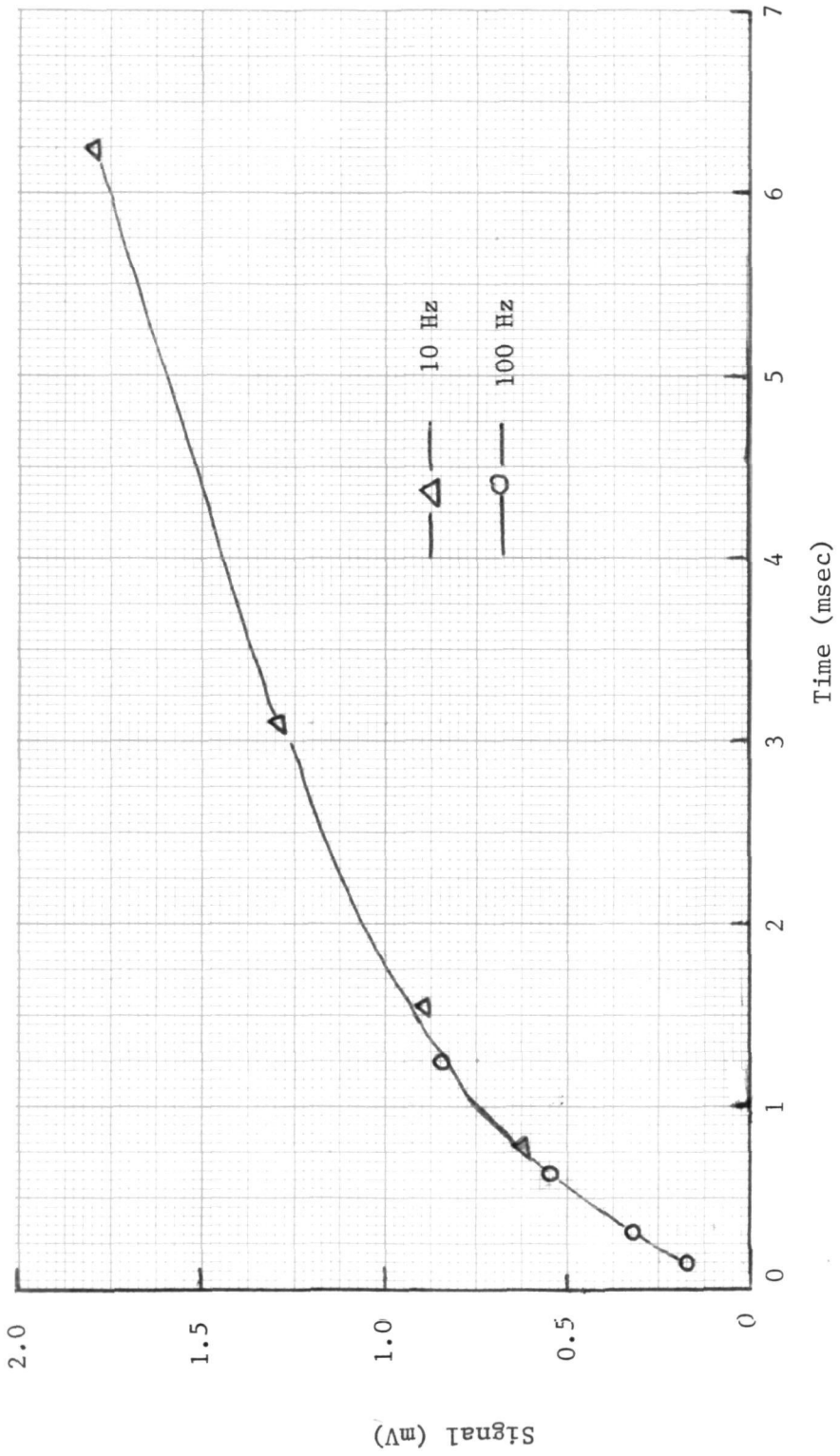

FIGURE 12 SSPC SIGNAL AMPLITUDE AS A FUNCTION OF INTEGRATION TIME

this flux level. The bending of the curve suggests that, at this flux level, the input may be saturating. However, the signal voltage is only a tiny fraction of the applied bias and is consequently too small to cause any saturation.

Section 5

AMCID TESTS

The test setup for the AMCID is shown in Figure 13A. During the integration period the bias has a store voltage applied (negative for p-type substrate) which collects the photo-generated carriers under the insulated gate. At the end of the integration period a short read pulse of approximately 10 μsec injects the collected charge back into the substrate and is read out through the source follower. This is shown in Figure 13B. The output signal is made of two components, a displacement current, which charges the AMCID capacitance, C, and the photo current. Just before the read pulse, the sample-and-hold circuit is zero restored by S1. Just after the read pulse, the signal is sampled by S2. The output of the sample-and-hold circuit is the value of the signal, i.e., the collected photo-generated charge, q, divided by the effective input capacitance, C_2, of the source follower:

$$S = \frac{q}{C_2} \times \frac{C_1}{C_1+C_2}$$

Five CID gates were examined. The bias, called store-and-read voltage ($V_{S/R}$), was varied between $\pm$1 volt and $\pm$6 volts. The negative read pulse was applied for approximately 10 microseconds at the end of each integration interval and the samples were taken immediately before and after the read pulse. The applied signal flux was a 20-Hz square wave of approximately 3×10^{10} photons/cm^2-sec.

Figure 14 shows the resulting waveforms for $V_{S/R} = \pm 1$ and ± 5 volts. Figure 15 plots the peak-to-peak value of the signal over the whole range of store-and-read voltages. Except for the -1 volt read voltage, there is only a slight indication of saturation at the higher voltages.

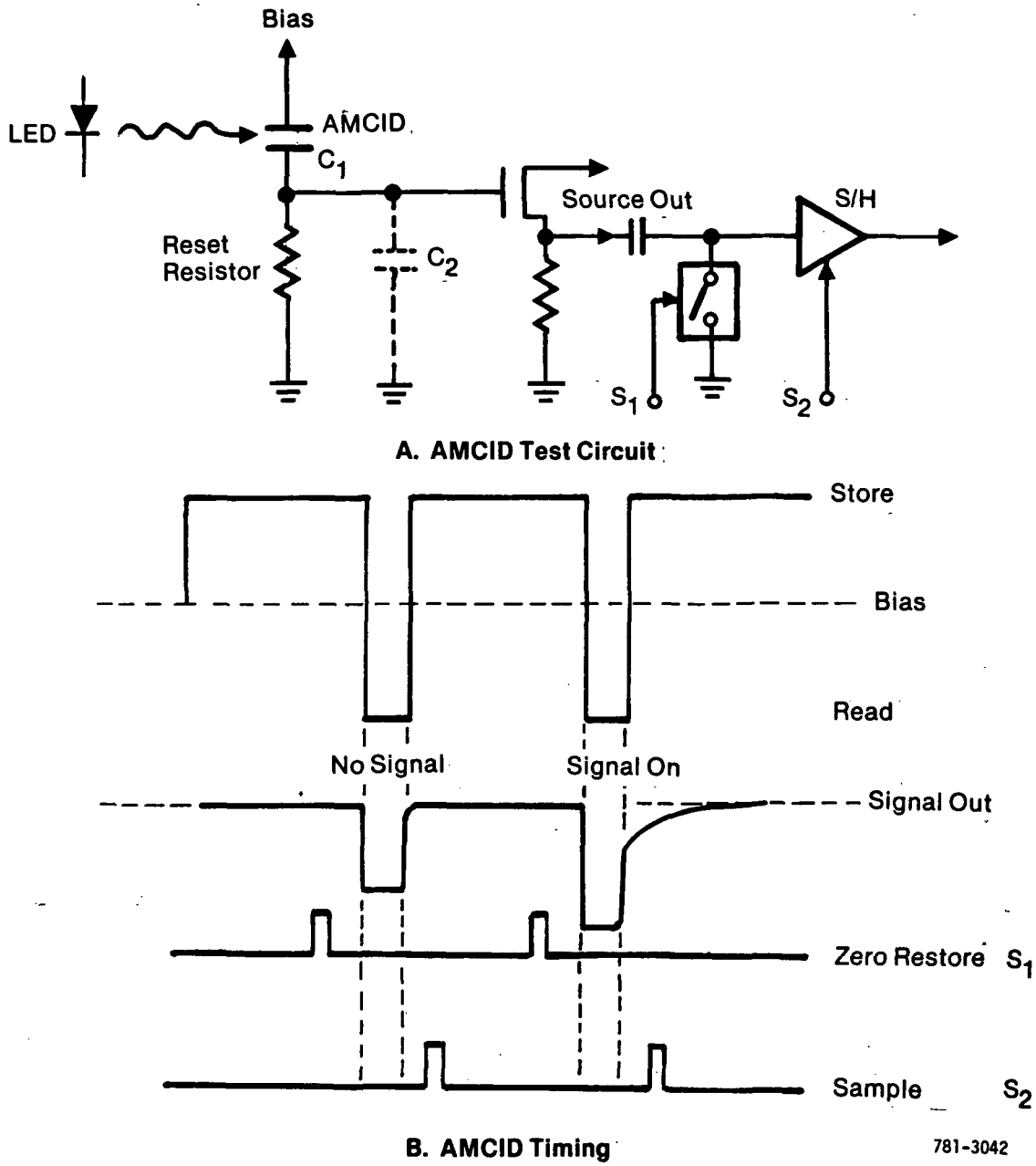

FIGURE 13 AMCID TEST SETUP

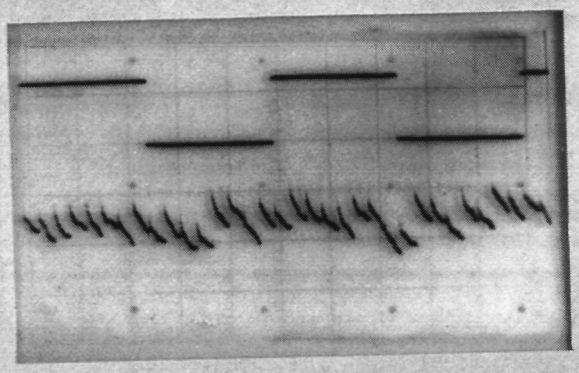

A. $V_{S/R}$ = +1 volt

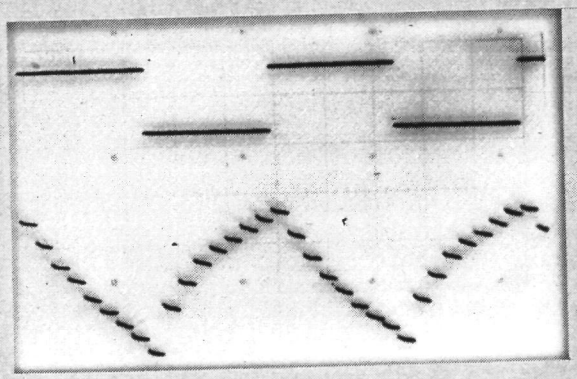

B. $V_{S/R}$ = +5 volts

FIGURE [illegible] AMOUNT OF SIGNAL WAVEFORMS FOR STORE-AND-READ VOLTAGES OF

ANT Horizontal Scale = 20 msec/div

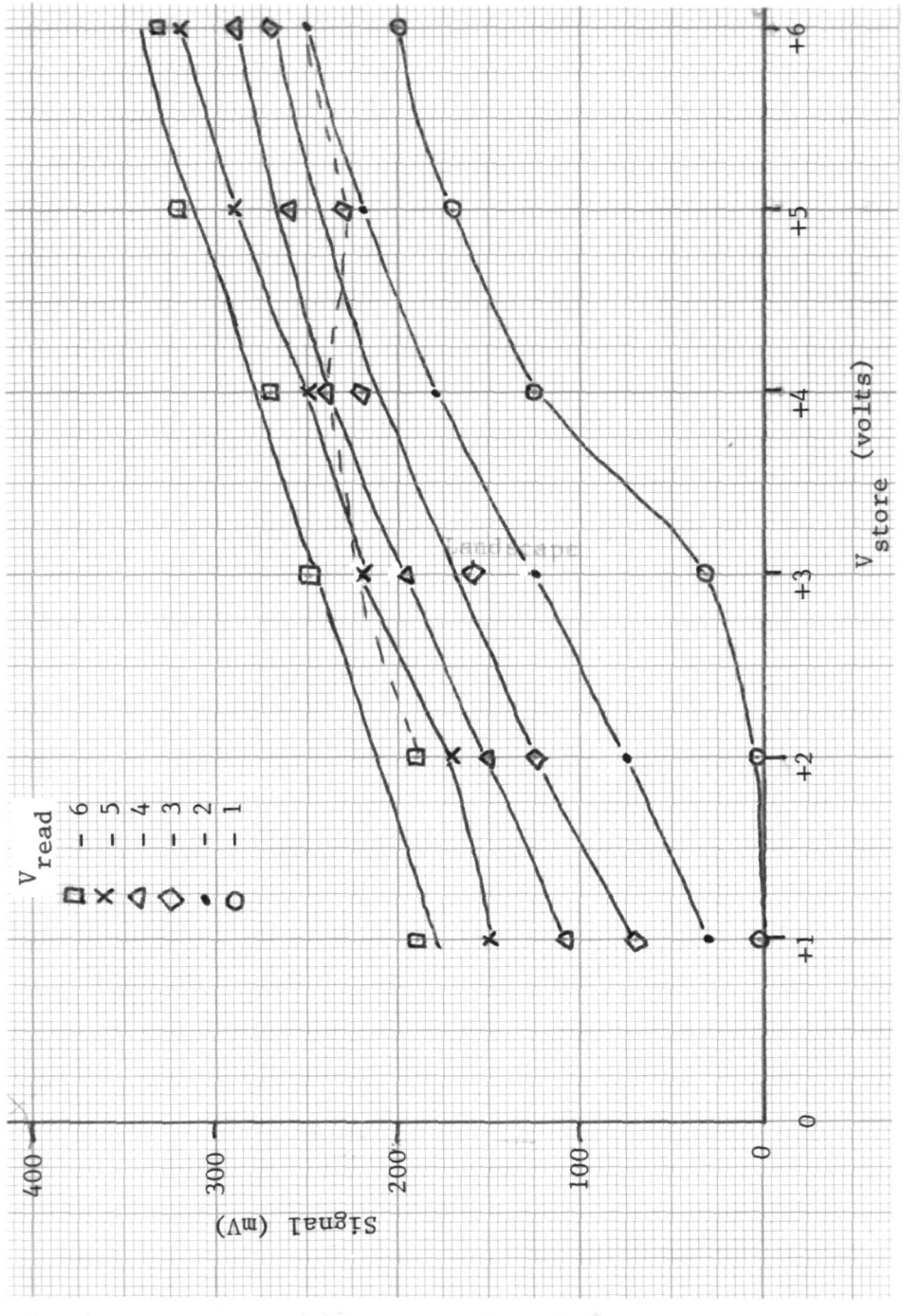

FIGURE 15 PEAK-TO-PEAK SIGNAL VS STORE-AND-READ VOLTAGES ON AMCID GATE

Studies of silicon devices at AESC have shown that the signal out appears to depend mainly on the difference between the store-and-read voltages. The dashed line in Figure 15 shows how the signal varies with $V_{S/R}$ for a constant difference of 8 volts (+6 to -2, +5 to -3, etc.). The figure shows that the signal is roughly constant over this range; thus, germanium appears to behave the same as silicon in this respect.

At a photon flux of 3×10^{10} ph/cm^2-sec, the signal varies linearly with integration time. The output of an AMCID gate with a 10-Hz square-wave flux applied was measured at several sample rates--i.e., from 8 to 128 samples per signal period (meaning integration times from 78 microseconds to 12.5 milliseconds). The resulting waveforms are shown in Figure 16; the root-mean-square signal level as measured by a wave analyzer is plotted in Figure 17.

Figure 16 illustrates another characteristic of the germanium AMCID that is also observed in silicon. The leading edge of the sampled waveform is very slow compared with that of the PC or the SSPC. This appears to be universal in the AMCID detector, and the phenomenon has been called the "slow rise".

The slow rise is evident at all the sample rates. Experimental and theoretical studies for silicon devices have indicated that it probably results from "bulk" trapping states in the detector material. It is probably not feasible to reduce the bulk traps to a sufficiently low level to eliminate the effect. The phenomenon can severely impact performance at high frequencies--resulting, for example, in background dependent bandwidth, nonlinearity and large responsivity variations across arrays. However, for very-low-signal applications requiring very long integration times (of the order of seconds), the slow rise may not represent a particular problem.

Figure 18 shows a noise spectrum for $V_{S/R} = \pm 1$ and ± 5 volts, with the sample-and-hold (S/H) input shorted. The noise levels are about a factor of 5 above those expected of a state-of-the-art silicon detector and readout electronics system, and would limit the sensitivity to about 600 electrons per sample.

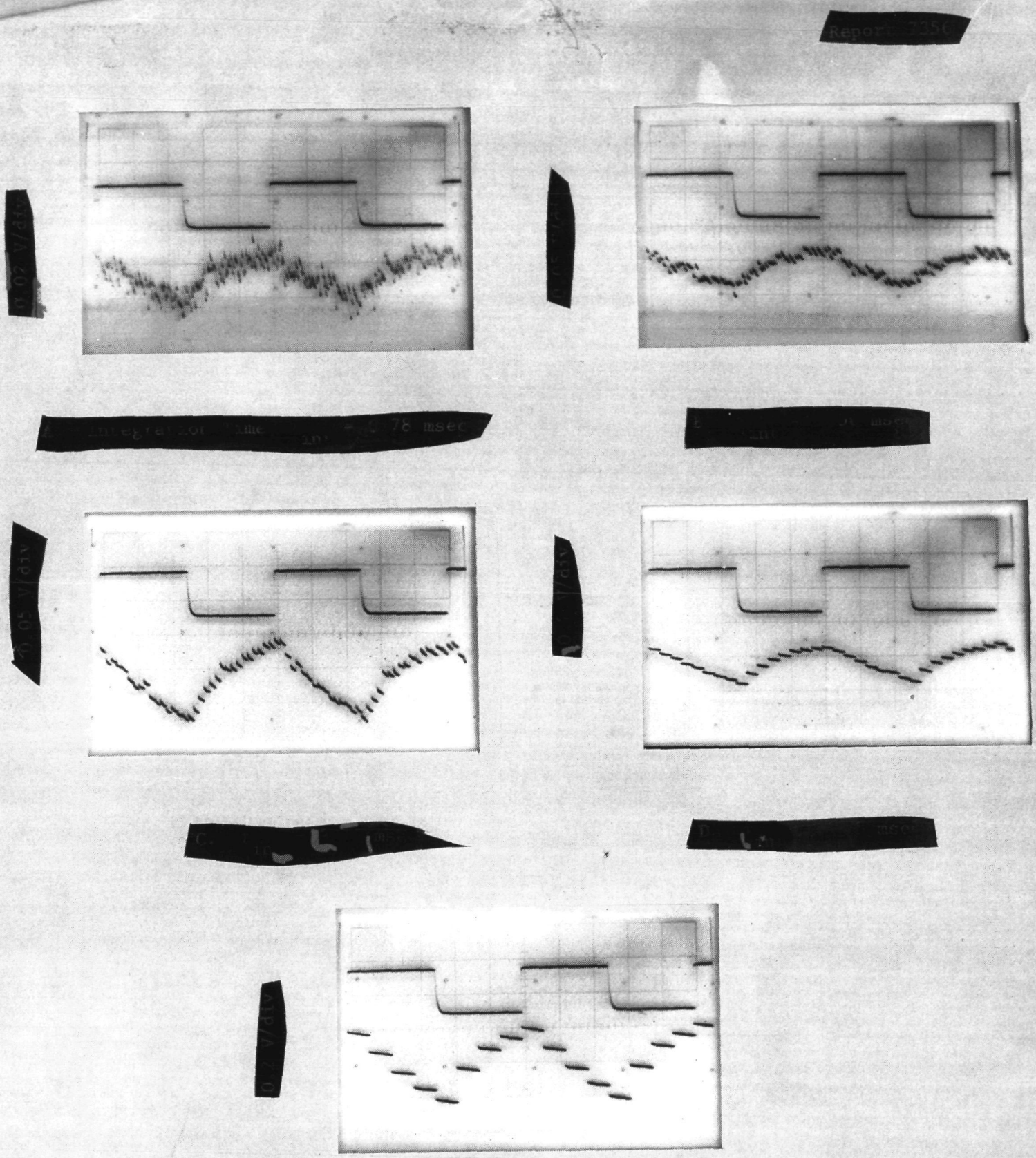

FIGURE 16 AMCID OUTPUT SIGNAL AS A FUNCTION OF INTEGRATION TIME
(Horizontal Scale = 20 msec/div)

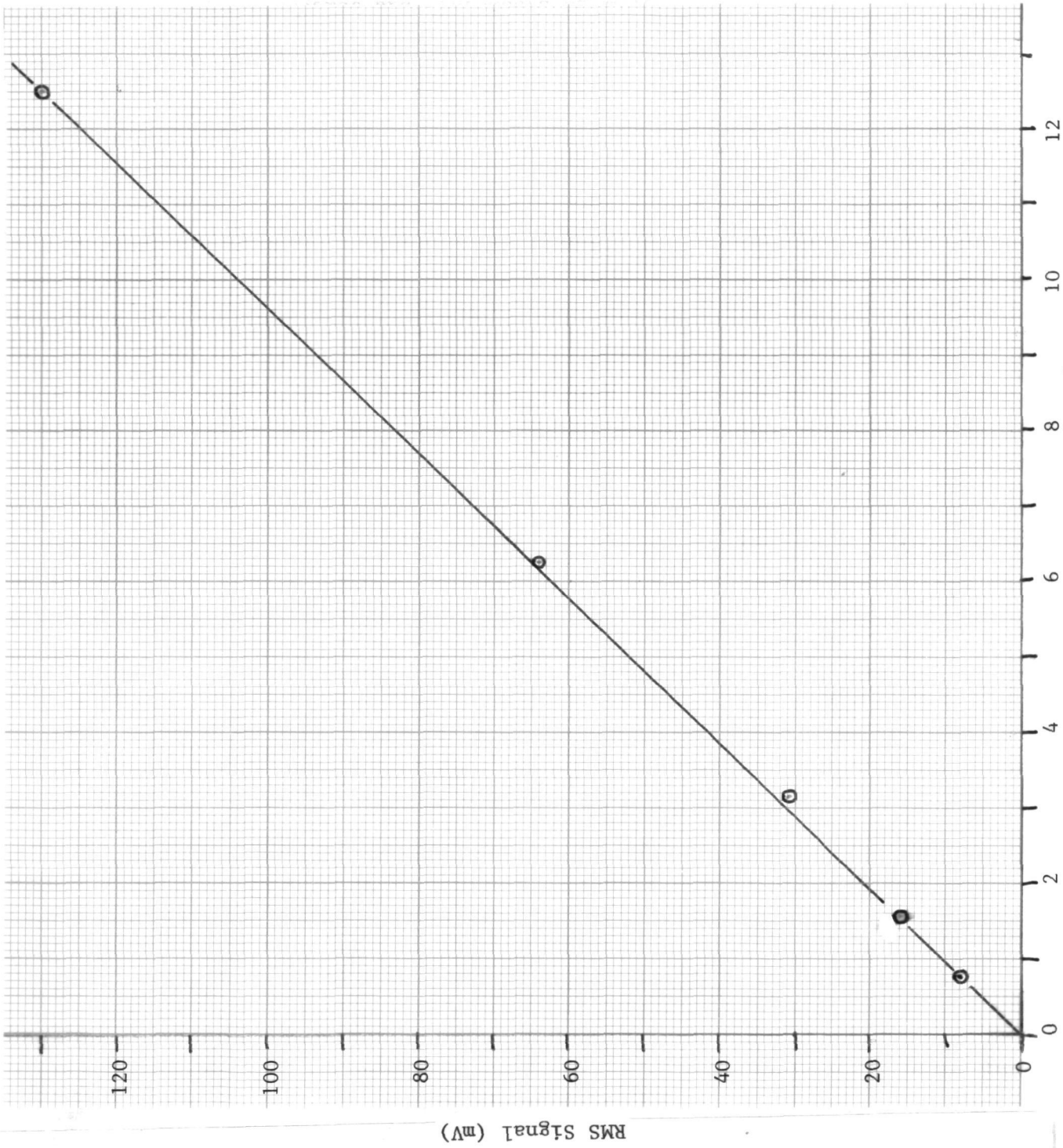

FIGURE 17 SIGNAL VS INTEGRATION TIME FOR AMCID

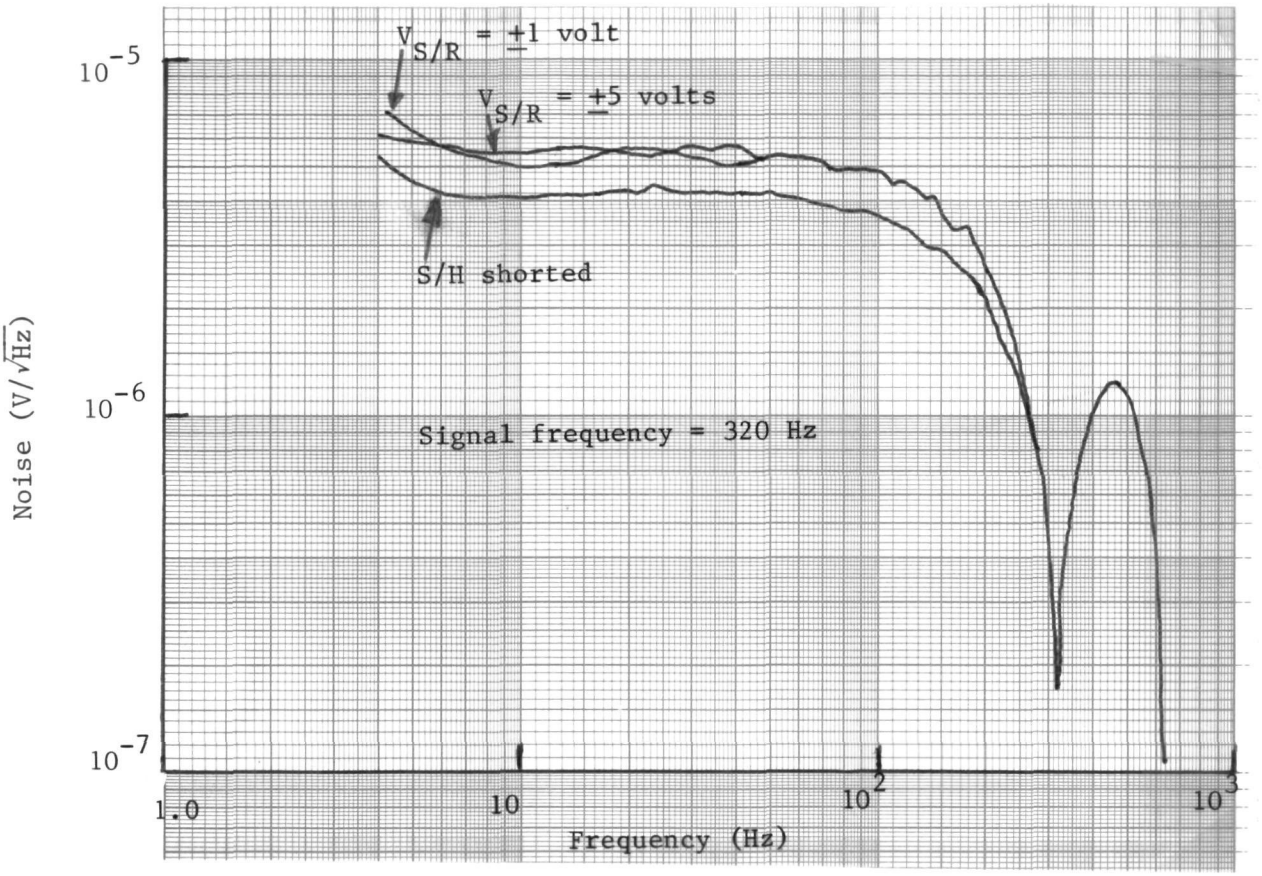

FIGURE 18 AMCID NOISE SPECTRA

Multiple time constants begin to become evident at higher signal fluxes (ϕ_s). Figure 19 shows the signal variation with a flux of 3×10^{10} to 3×10^{12} ph/cm^2-sec. At higher sample rates, these effects should be reduced.

FIGURE 19 AMCID SIGNAL WAVEFORM AS A FUNCTION OF SIGNAL FLUX
(Horizontal Scale = 20 msec/div)

Section 6

CONCLUSIONS AND RECOMMENDATIONS

During this program the feasibility of fabricating the AMCID in germanium was established. AMCID operation was successfully demonstrated for devices configured in wafers of mercury doped-germanium and using Al_2O_3 as an insulator. There is no reason to believe that they can not be fabricated equally well on gallium doped-germanium. However, it was found that the germanium AMCIDs exhibited a "slow rise" characteristic. A similar phenomenon leads to nonlinear response and background dependent bandwidth in silicon AMCID and is believed to be due to unavoidable bulk traps. Consequently, attention was directed to demonstrating an alternative switched-sampled-photoconductor approach for mosaic readout. The SSPC will also perform satisfactorily at low frequencies, but will exhibit the same kinds of response nonlinearities as the conventional photoconductor due to dielectric relaxation at high frequencies. Both the AMCID and the SSPC will work for long integration times when these nonlinear effects may be irrelevant.

Aerojet recommends that development of the switched sampled photoconductor, fabricated as a hybrid structure with detectors "bumped" to silicon MOS switching and preamplifier electronics be persued as the optimum architecture for a VLWIR germanium mosaic focal plane. The SSPC approach will make maximum use of existing technology, offers the greatest flexibility, and represents a lower risk than the AMCID with no loss of either present or theoretical maximum performance.

REFERENCES

1. L. L. Chang and H. N. Yu, "The Germanium Insulated-Gate Field Effect Transistor", Proc. IEEE, p. 316, March 1965.

2. S. Iwauchi and T. Tanaka, "Interface Properties of Al_2O_3-Ge Structure and Characteristics of Al_2O_3-Ge MOS Transistors", Jap. J. Appl. Phys., 10, N2, p. 260 (1971).

3. D. K. Schroder, "A Two-Phase Germanium Charge-Coupled Device," App. Phys. Let., 25, N12, p. 747 (1974).

4. K. L. Wang and P. V. Gray, "Fabrication and Characterization of Germanium Ion-Implanted IGFETs", IEEE Trans. on Elec. Devices, p. 353, June 1975.

5. Kvon Ze Don, I. G. Neizvestnyy, V. N. Ovsyuk, and A. V. Rzhanov, Germanium MOS-Transistor, NASA Technical Manual TM-75902, January 1981.

6. Kvon Ze Don and I. G. Neizvestnyy, Weak Inversion Mode in Germanium MOS-Transistor, NASA TM-75903, January 1981.

7. E. E. Haller, Ge:Ga Far Infrared Photoconductors, Lawrence Berkeley Laboratory, University of California, Progress Report May 1 to December 31, 1979.

8. James Yee, Stressed Gallium Doped Germanium Detector, AESC Final Report under Contract NAS5-25975 for NASA Goddard Space Flight Center, July 1980.

9. C. M. Parry, Cryogenic Switched MOSFET Characterization, AESC Report 7165 for NASA Ames Research Center, March 1981.